



HAL
open science

Morphological impact of insulator on inkjet-printed transistor

Sjeung Jae Moon, Malo Robin, Kuai Wenlin, Molard Yann, Byung Seong Bae, Tayeb Mohammed-Brahim, Emmanuel Jacques, Maxime Harnois

► **To cite this version:**

Sjeung Jae Moon, Malo Robin, Kuai Wenlin, Molard Yann, Byung Seong Bae, et al.. Morphological impact of insulator on inkjet-printed transistor. *Flexible and Printed Electronics*, 2017, 2 (3), pp.035008. 10.1088/2058-8585/aa8760 . hal-01622463

HAL Id: hal-01622463

<https://univ-rennes.hal.science/hal-01622463>

Submitted on 24 Oct 2017

HAL is a multi-disciplinary open access archive for the deposit and dissemination of scientific research documents, whether they are published or not. The documents may come from teaching and research institutions in France or abroad, or from public or private research centers.

L'archive ouverte pluridisciplinaire **HAL**, est destinée au dépôt et à la diffusion de documents scientifiques de niveau recherche, publiés ou non, émanant des établissements d'enseignement et de recherche français ou étrangers, des laboratoires publics ou privés.

Morphological impact of insulator on inkjet-printed transistor.

Sjeung Jae Moon,^{1, 2} Malo Robin,^{1, 3} Kuai Wenlin,¹ Molard Yann,³ Byung Seong Bae,² Tayeb Mohammed-Brahim,¹ Emmanuel Jacques,^{1, *} Maxime Harnois,^{1, *}

¹ *Institut d'Électronique et des Télécommunications de Rennes, Université Rennes 1, UMR CNRS 6164, Campus de Beaulieu, 35042 Rennes Cedex, France*

² *Department of Display Engineering, Hoseo University, Asan, Chungnam 336-795, Republic of Korea*

³ *Institut des Sciences Chimiques de Rennes, Université de Rennes 1, CNRS UMR 6226, Rennes, France*

Abstract:

This study reports on the impact of electrodes (source and drain) and insulator cross-sectional profile on the electrical behavior of printed organic field effect transistors (OFET). Varying processing technique from classical lithography to inkjet printing shows different cross-sectional profile. Indeed, due to coffee stain effect (usually considered as a drawback), inkjet-printed insulator shows wave-shaped profile although spin-coated one is perfectly smooth. However, OFET electrical behavior is not drastically impacted by insulator cross-sectional profile. Moreover, this study clearly demonstrates that independently of insulator cross sectional profile, OFET fabricated with printed-electrodes shows the worst electrical characteristics. Consequently, this work clearly demonstrates that a challenging issue for the fabrication of efficient fully-printed OFET relies on drain and source optimization (morphology or material for instance).

Printed Electronics (PE) has gained a growing interest throughout the past decade.^[1] Consequently, many techniques such as: screen printing,^[2] roll to roll,^[3] inkjet printing,^[4, 5, 6] ... have been considered. One of them, the Drop on Demand (DoD) inkjet printing technique, allows very small amount of liquid deposition (1-100pl) at high throughput and high accuracy on various kind of substrates.^[1] Moreover, the DoD technology benefits from material deposition only at the desired location (i.e., maskless additive patterning) reducing materials consumption compared to lithography technique (i.e., patterns fabricated using mask and etching process). Those interesting properties will promote organic electronic (OE) production on non-conventional substrates such as flexible or biodegradable substrates. Indeed, most of organic electronic devices such as: Organic Light Emitting Diode (OLED),^[7] Solar Cells (SC)^[8] and Organic Field Effect Transistor (OFET)^[9, 10] can be fabricated using functional printable ink.

Inkjet printing technology requires multidisciplinary skills and consequently many challenging topics, such as: i) functional inks formulation,^[11] ii) jetting optimization,^[12] iii) fluid drying control,^[13] iv) devices fabrication and characterization, etc.^[10, 14]. All these challenges must be addressed before reliable fabrication of fully-printed devices. Thus, literature is replete with experimental works dealing with OFET electrical characteristics improvements using inkjet printing technology. In most cases, works focus on: new printable materials (i.e., organic semiconductors (OSC), insulators, conductive),^[15, 16, 17] new semiconductor crystallization process^[18]... and experiments are often performed on non-fully-printed OFET structures (smooth insulator and/or drain and source electrodes fabricated using lithography technique) which offers better morphological characteristics than fully-printed ones. These studies are necessary but have to be completed with others dealing with deeper investigations on fully-printed OFET structures themselves.

A relevant study has highlighted the morphological impact of printed gate electrode in bottom gate-bottom contact OFET. It has been shown that optimization of the gate electrodes profile (i.e., from convex to concave) strongly reduces OFET leakage current (I_G).^[20] This study has paved the way to others, which have to report on morphological impact of the other layers (insulator and/or source and drain electrodes) on OFET electrical behavior. Consequently, in this work and for the first time, the effect of smooth polymeric insulator and wave-shaped printed insulator on OFET electrical behavior have been study. Such systematic study has been performed using printed silver as drain and source electrodes in the first section and thermally evaporated gold in the second one. Note that, these materials have been chosen according to the literature. Indeed, silver and gold are the most frequently reported materials using inkjet printing and thermal evaporation, respectively.

Results and discussion

DoD inkjet printing technique is based on the coalescence of printed droplets usually composed of solvent and solute (e.g, nanoparticles, polymers...) to form complex patterns after drying. As extensively described since Deegan observations,^[19] a droplet of liquid is subject to the well-known phenomenon called: “coffee stain effect” which results from a greater evaporation rates at the surrounding of “the triple contact line”. Consequently, when the triple line is pinned, solute transport from the center to the edge is induced by replenish flow. This mechanism leads to non-uniform films morphology after complete solvent evaporation. Reducing the coffee stain effect is still a challenge to overcome in the field of DoD technology. Indeed, it requires complex: i) techniques development,^[20, 21] ii) ink formulation,^[10, 22] iii) printing parameters optimization^[10]... in order to obtain a profile as smooth as possible. Moreover, OFET is a multi-layers printed structure, it seems evident that each layer will induce additional disturbances during drying step. Consequently, questions have to be answer: What is the impact of drying interactions between stacked layers on the OFET electrical characteristics? Is it mandatory to perform smooth insulator profile in order to fabricate electrically efficient fully-printed OFET? Which layer (insulator or electrodes) is the key parameter impacting OFET electrical behavior? Note that, the two last questions are particularly crucial for bottom gate OFET.

In order to determine such impacts, comparative studies have been performed between: insulating films that are spin coated or inkjet-printed.

a Inkjet-printed source and drain electrodes

i) Processing and morphological study

As shown in **figure 1** and more detailed in experimental section, bottom gate-bottom contacts structure has been used to fabricate transistors in order to answer previously mentioned questions. Insulator process variants (spin-coated or printed insulator) have been performed in order to highlight if insulator processing techniques have a strong impact on OFET fabrication and electrical behaviors. Process variants are shown in figure 1 and can be described as follows:

Gate electrodes have been inkjet-printed using silver ink for all OFETs (**figure 1a**). As the effect of this step have already been extensively study,^[20] the gate process was not changed in this study. After this step, insulator has been performed using two different techniques: spin coating (**figure 1b**) and inkjet printing (**figure 1c**). Epoxy based photoresist (Su8-2000 series; MicroChem, Westborough®, MA, USA) has been used as insulator because it has already demonstrated interesting insulating properties in many applications independently of fabrication

techniques such as deep coating, spin coating and inkjet printing.^[28, 29, 10] Moreover, epoxy based insulators show low temperature processing (i.e. <100°C), good chemical resistance, low leakage current density, dielectric constant about 3,^[10, 30] high breakdown electric field (evaluated at 3 mV.cm⁻¹) and interesting wetting behavior. Indeed the hydrophobicity of insulator influences the OFET electrical behavior as demonstrated in^[31] where the more the hydrophobicity was, the more the field effect value was.

Inkjet-printing insulator requires more experimental parameters adjustment than spin-coated one. Indeed, DoD technology needs much more parameters optimization than spin coating. Both technics need accurate control of the substrate temperature. However, DoD processing is particularly dependent of the : i) nozzles size, ii) number of nozzles used at the same time during printing, iii) jetting frequency, iv) jetting waveform (see **figure S1** in supplementary file), v) drops overlapping.... Here, substrate temperature, nozzles size, activated nozzles number and jetting frequency have been kept constant at 50°C, 21µm, 16 and 1 KHz, respectively. Jetting parameters are detailed in supplementary file (see **figure S1**) and have also been kept constant. Those parameters have been experimentally optimized in order to respect jettable criterions (see experimental section) and perfect droplet printing behavior has been obtained (see in **movie S1**).^[10, 12] Moreover, epoxy based ink has been also used for its versatility because it is a low-molecular-weight based ink (7 KDa). Indeed, this ink can be easily printed without well-known jetting drawbacks (e.g., satellites droplets, long lived filaments, etc) as shown in movie S1.^[10] Note that, ink composition and rheological parameters are detailed in experimental section. Overlapping parameter will be discussed deeply in the following section.

As shown in **figure 1d** and **1e**, source and drain electrodes have been inkjet-printed for both insulator configurations. Fullerene (C60) has been chosen as semiconductor because it is an extensively studied material giving relatively high field effect mobility^[32] and because it allows to fabricate N-type OFETs that are less studied in the literature. In the field of PE, the fabrication of fully-printed transistors as well as circuits is the ultimate goal. However, it is well known that transistors fabricated using solution-processed semiconductors often show less accurate results (i.e., more electrical characteristics dispersions) than evaporated ones. Indeed, using solution-processed semiconductor, crystals did not grow in the same direction leading to increase the dispersion of OFET electrical characteristics. Those statements justify using thermally evaporated semiconductor in order to study accurately the transistor electrical behavior in function of insulator morphologies and drain-source electrodes processing technics.

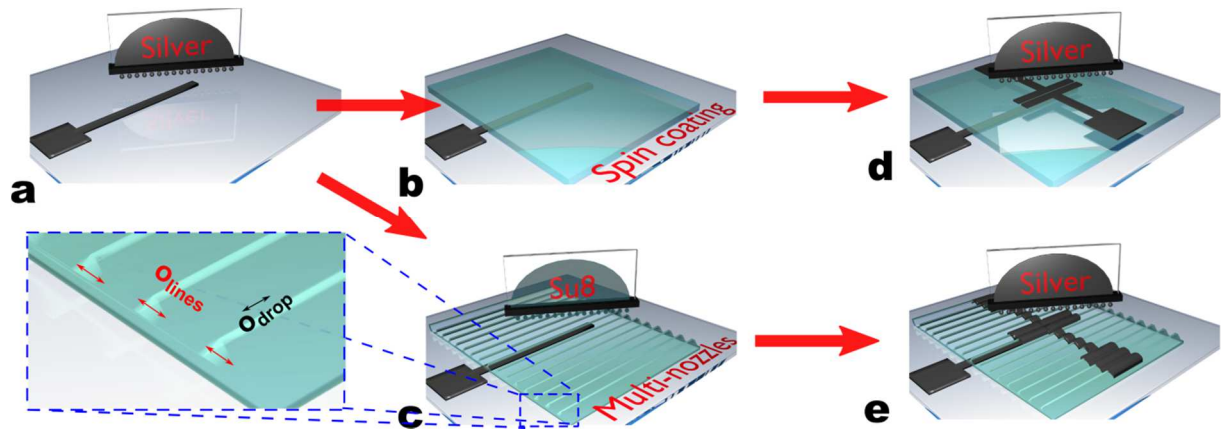


Figure 1: OFET Fabrication steps including the variant steps for insulator fabrication. a) gate inkjet printing using silver nanoparticles based ink, b) spin coating insulator (Su8-2000.5 photoresist), c) Inkjet-printed insulator (Su8-2000.5 based ink), d) Inkjet-printed Source and drain electrodes (silver) on spin-coated insulator, e) Inkjet-printed Source and drain electrodes (silver) on inkjet-printed insulator. Note that, only insulator profile varies for this set of experiments.

As shown in **figure 1b**, **1c** and in **figure 2**, two different insulators morphologies have been performed. As published in another work,^[20] a smooth insulator surface has been obtained using spin coating technique onto printed gate (**figure 2a and 2d**). In this case, Centrifugal force induces fast drying time that avoids the impact of printed gate profile on insulator morphology. Moreover, well-defined sources and drain electrodes (**figure 2c and 2d**) have been fabricated on spin coated Su-8 exposed to UV-ozone (see in experimental section).

Printed insulator shows wave-shaped profile mainly due to coffee stain effect (**figure 2b and 2f**). This phenomenon has been extensively explained in a previous study and can be briefly summarized as follows.^[10] Droplets coalescence along x axis forms one line and line coalescence along y axis forms the film. The lines are formed independently of each other and the evolution of the wavy shaped profile is due to the local coffee ring effect. Height of peaks and valley are mainly governed by overlapping distance (O_{lines}) between adjacent lines (Zoom in **figure 1c**) and by overlapping distance (O_{drop}) between adjacent droplets.

Concerning drain and source electrodes, results reported in figure 2, contrast with previous studies that have shown a dewetting effect of printed material on top of wavy structures.^[33, 34, 35] Indeed, results of **figure 2 b**, **2e**, **2f** and OFET optical pictures (see figure S2 in supplementary file) show that even if insulator profile are strongly buckled (i.e, more than $2\mu\text{m}$ height between the maximum & minimum values) drain-source electrodes are well defined (3D profiles are shown in figure S2). It signifies that chemically modified (OH groups appear due to UV-Ozone

exposure) epoxy thin film offers the possibility to pin inkjet-printed silver ink. These results can be explained by the high contact-angle hysteresis value of epoxy thin film exposed to UV-ozone.

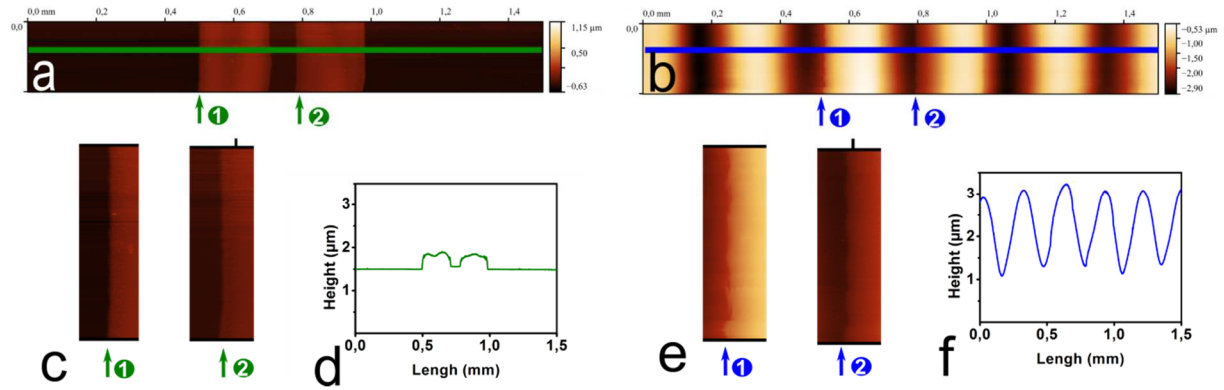


Figure 2: Morphological behavior of spin-coated devices and Inkjet-printed devices. Top view scan (1.5mm*200μm) of drain and source electrodes fabricated on: a) spin-coated Su-8 insulator and b) inkjet-printed Su-8; c) zoom on spin-coated insulator showing left side of inkjet-printed drain and source electrodes which are marked 1 and 2, respectively; d) Cross section along x axis of drain-source electrodes fabricated on spin-coated insulator; e) zoom on inkjet-printed insulator showing left side of inkjet-printed drain and source electrodes which are marked 1 and 2, respectively; f) Cross section along x axis of drain-source electrodes fabricated on inkjet-printed insulator. Note that 3D profiles of printed layers is shown in figure S2b.

ii) Electrical study

Figure 3 shows transfer characteristics of OFETs using spin coated or inkjet-printed insulator. Moreover, relevant electrical parameters are summarized in **table 1**. Data shown in **Figure 3a** is relative to spin coated devices and **Figure 3b** is relative to inkjet-printed devices. V_{GS} has been swept from -20 to 60 V with $V_{DS} = 20$ V. Figures shows the transfer characteristics of 5 same size OFETS fabricated on the same substrate. The common channel length L and width W is equal to 100 μm and 5000 μm, respectively. For each transistor, the Subthreshold slope SS is calculated from the invert of the maximum slope of the drain current in logarithm scale as a function of the gate voltage in the subthreshold regime. The Threshold Voltage (V_{TH}) and the field effect mobility are calculated using the Y-function method established for silicon MOSFETs.^[36] It has been established as a simple but powerful method to calculate low-field effect mobility, threshold voltage and contact resistance.

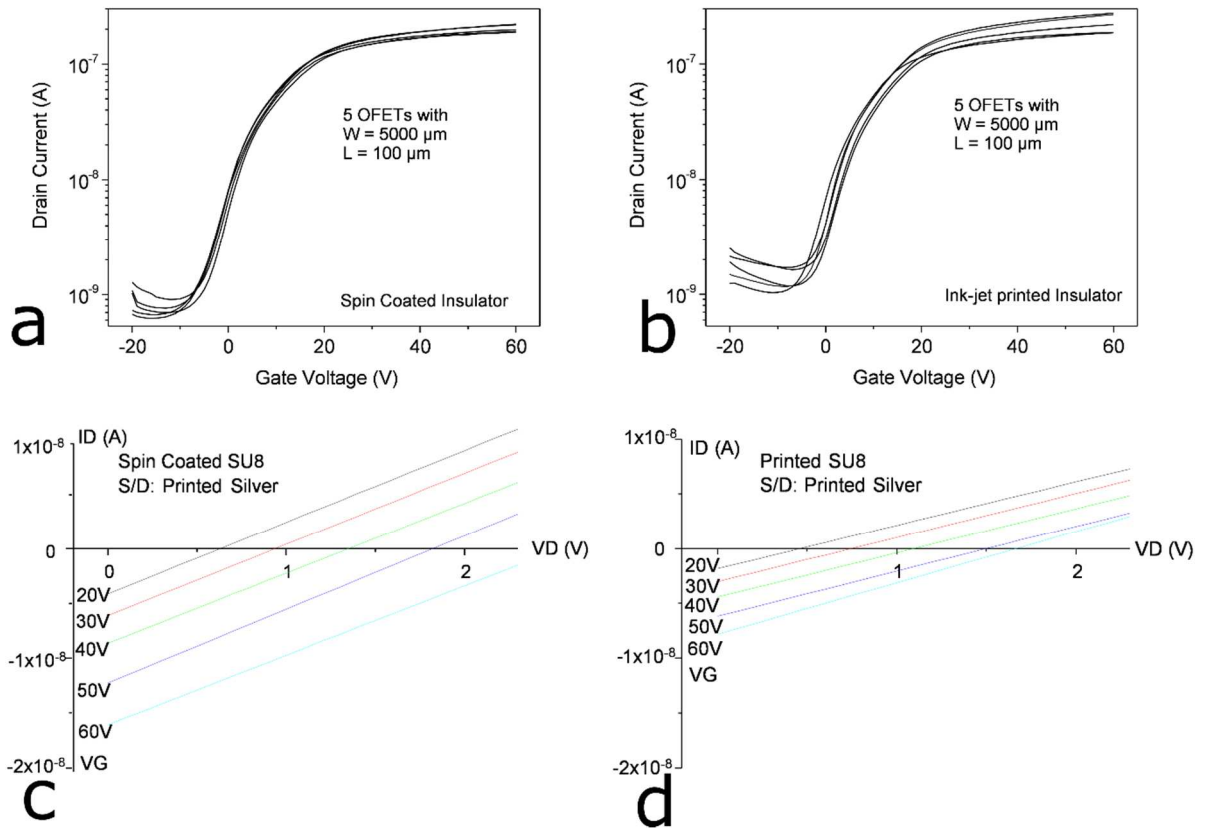


Figure 3: OFET transfer characteristics as a function of insulator fabrication with inkjet-printed source and drain electrodes. Transfer characteristics of five devices for: a) spin-coated insulator; b) Inkjet-printed insulator. Output Characteristics at low values of the drain-source voltage V_{DS} of OFETS for c) spin-coated Su8 and printed source and drain electrodes; d) printed Su8 and printed source and drain electrodes.

Processing Technique		W/L ($\mu\text{m}/\mu\text{m}$)	Insulator thickness in μm	μ_0 ($\text{cm}^2 \cdot \text{V}^{-1} \cdot \text{s}^{-1}$)	V_{TH} (V)	SS (V/dec.)	R_c (Ω)	V_{DS} (V)
Spin	Average	5000/100	1.5	$1.2 \cdot 10^{-2}$	8	6.5	$6.5 \cdot 10^7$	20
	Stand. Dev.	--	--	$4 \cdot 10^{-3}$	1.2	0.3	$2 \cdot 10^7$	--
IJP	Average	5000/100	1.7	$7.4 \cdot 10^{-3}$	9	6.5	$6.9 \cdot 10^7$	20
	Stand. Dev.	--	--	$2 \cdot 10^{-3}$	2.8	0.2	$1.8 \cdot 10^7$	--

Table 1: Summary of electrical parameters as a function of insulator processing techniques (spin coating and inkjet printing). Note that source and drain contacts are inkjet-printed silver. μ_0 , V_{TH} , subthreshold slope (SS) and contact resistance R_c are calculated using Y-function method.

Main electrical parameters calculated using Y-function method (detailed in supplementary file) are summarized in table 1 in order to compare the effect of insulator processing techniques (spin-coated or inkjet-printed). Results, depicted in table 1, don't show clear tendency between the following electrical parameters: threshold voltage, subthreshold slope and contact resistances. Note that, the intrinsic mobility μ_0 seems a little bit higher for spin-coated insulator that could be correlated to the smoother insulator surface (see in figure S3). In conclusion, the global OFET behavior is not strongly dependent of insulator processing techniques. It signifies that, even if buckled insulator profile occurs (see in figure 2) using inkjet printing technology, it doesn't drastically impact electrical OFET behavior.

The other parameter to check is the gate leakage current that cannot be negligible when using organic insulator and not silicon dioxide or alumina as usual. An original way to study the gate leakage is to make a zoom on the starting output characteristics of the OFETs at low values of the drain-source voltage V_{DS} .

At very low V_{DS} , the drain current starts from negative values for N-type OFETs as shown in figure 3a and 3b where the output characteristics are plotted at very low V_{DS} values for the two types of OFETs. The starting negative value of the drain current I_D is more and more negative when the gate voltage V_{GS} is more and more positive. For the same value of V_{GS} , the starting value of I_D is more important for spin-coated SU8 OFETs than for printed SU8 ones.

Such behavior are usual when the leakage current through the gate insulator is important. It can be explained considering the scheme of bottom-gate bottom contacts N-type OFET presented in figure 4.

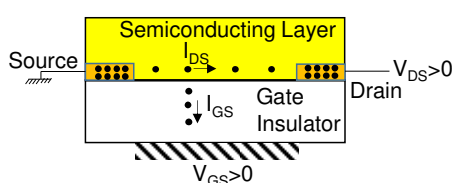


Figure 4: Scheme of N-type OFET showing the drain-source current I_{DS} and the gate-source current I_G .

At very low value of V_{DS} , the gate field due to V_{GS} is more important than the drain electric field due to V_{DS} . High number of electrons flow in the direction of the positively polarized gate. Due to this important flow, electrons flow in the semiconductor to compensate the loss of electrons in the channel, inducing negative drain-source current. When V_{DS} increases, drain-source electric field becomes more and more important inducing positive drain-source current. The V_{DS} value for which the drain current becomes positive occurs when drain-source electric field becomes higher than the gate electric field.

Following such explanation, higher the starting negative value of I_D is, higher the gate leakage current for the same gate-source voltage is. Figure 6 shows the starting negative drain current at V_{DS} closed to 0V as a function of the gate-source voltage for both types of OFETs. At very low gate-source voltage, drain current stays constant around 0. This means that the gate electric field is not strong enough to induce gate leakage current. When the gate-source voltage is large enough to induce such leakage current, the starting drain current is negative. It is more and more negative when the gate-source voltage increases. For spin-coated SU8, the negative drain current starts to increase a little bit earlier than the current of printed SU8 and its value is higher when increasing V_{GS} . Gate leakage current is then slightly higher in spin-coated SU8. More precisely, it is difficult to determine the origin of this leakage. Indeed, it can be due to the intrinsic properties of the spin-coated SU8 and also to the use of printed silver as gate contact and as source/drain contacts.

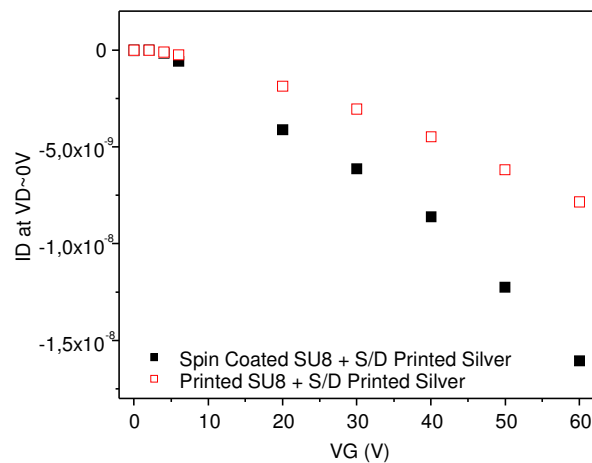


Figure 5: Starting negative drain current ($V_{DS}=0V$) as a function of gate-source voltage. This starting current is derived from the plot of output characteristics at different V_{GS} .

In conclusion, results have demonstrated that SU8 processing techniques doesn't show high impact on OFET electrical behavior even if OFET fabricated using spin-coated Su8 as gate insulator induces more gate leakage current. These results show that polymeric insulator fabricated using additive manufacturing techniques (e.g. IJP) is a good candidate in order to reach fully solution processed OFET. Indeed, with identical electrical behavior, there is no doubt that inkjet printing is mainly the most interesting technique for technological considerations. For instance, insulator deposition locally on the transistor gate will allow no electrical influence between transistors of the same circuits. Note that, other inkjet printing advantages, like low material consumption, has been previously described in the introduction section.

b Evaporated gold film as source and drain electrodes

Results of previous sections have shown moderate I_{on}/I_{off} ratio (approximately 2 decades) which is a limiting factor. Consequently, investigations have to be performed on drain and source contacts processing techniques. In this section, thermally evaporated gold is used as drain and source contacts. Indeed, most of relevant works dealing with non-fully solution processed OFET is performed using thermally evaporated gold as source and drain contacts. Moreover, same comparative study than in last sections, focusing on insulator processing techniques, is performed.

As described previously, printed silver gate is performed and SU8 is deposited by spin-coating or by printing (figures 6b and 6c). Then, source and drain electrodes (50nm thick) have been thermally evaporated (figures 6d and 6e).

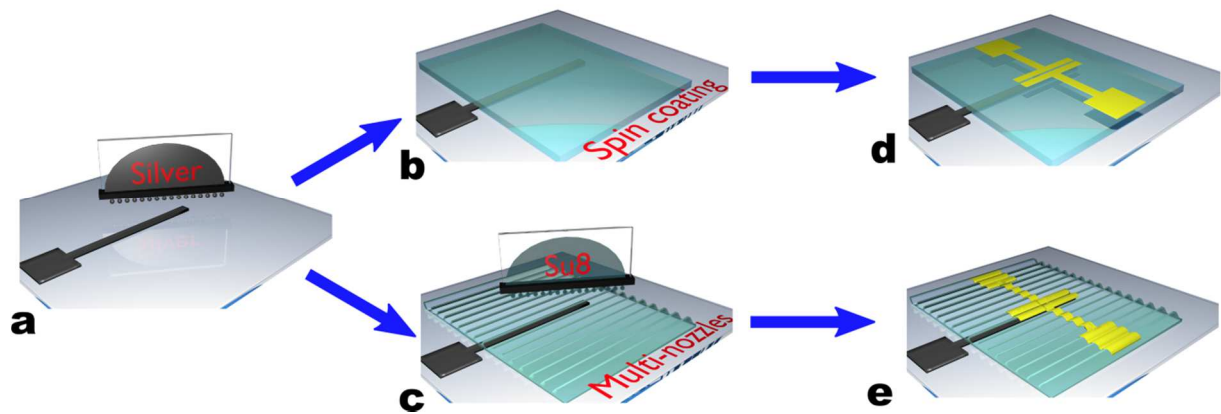


Figure 6: OFET Fabrication steps including the variant steps for insulator fabrication. a) gate inkjet printing using silver nanoparticles based ink, b) spin coating insulator (Su8-2000.5 photoresist), c) Inkjet-printed insulator (Su8-2000.5 based ink), d) Source and drain electrodes (gold) thermally evaporated on spin-coated insulator and patterned using lithographical process, e) Source and drain electrodes (gold) thermally evaporated on inkjet-printed insulator and patterned using lithographical process. Note that, only insulator profile varies for this set of experiments.

Figure 7 shows the transfer characteristics of five OFETs (similar size: 5000 μm channel width and 100 μm channel length) using spin-coated SU8 or printed SU8. **Table 2** shows the main OFET electrical parameters as function of insulator processing techniques.

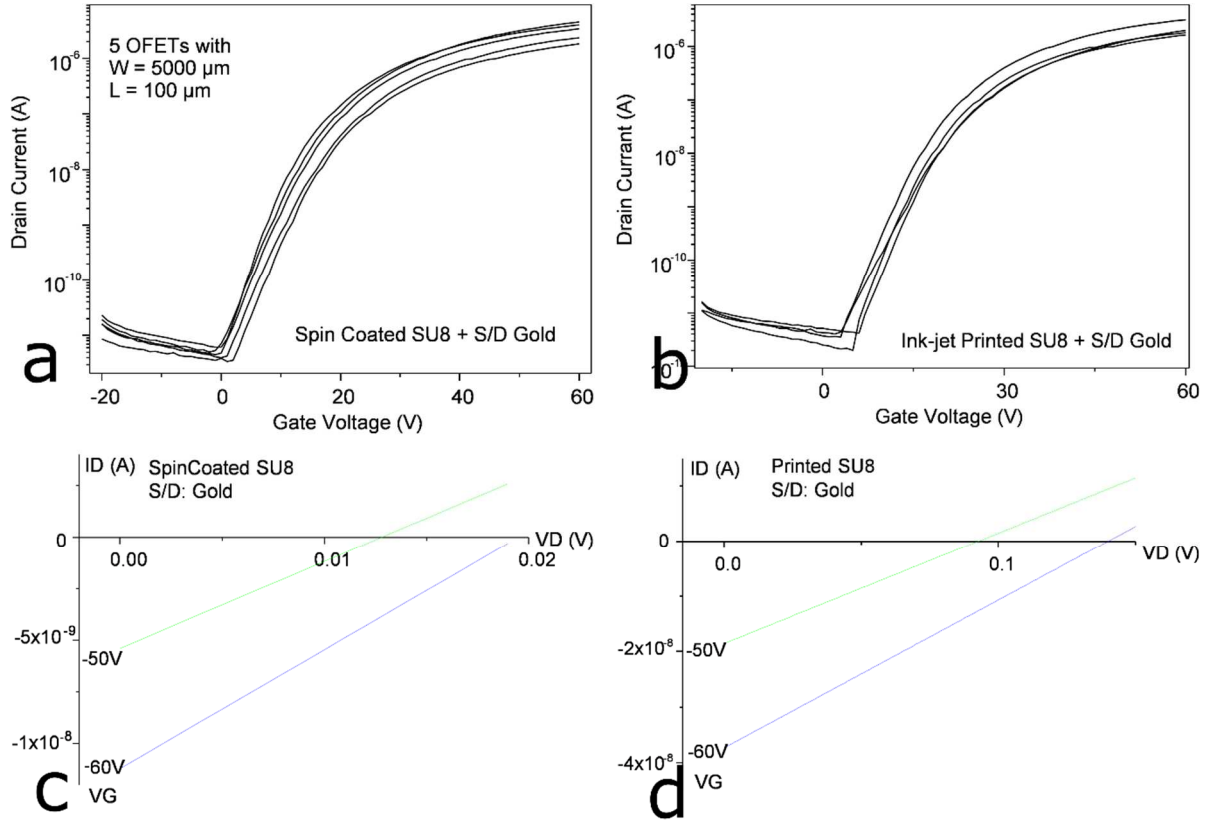


Figure 7: OFET transfer characteristics as a function of insulator fabrication with evaporated gold source and drain electrodes. a) Transfer characteristics of five similar size devices for spin-coated insulator, b) Transfer characteristics of five devices for Inkjet-printed insulator. Output Characteristics at low values of the drain-source voltage V_{DS} of OFETS for c) spin-coated Su8 and evaporated source and drain electrodes; d) printed Su8 and evaporated source and drain electrodes.

Transfer characteristics clearly show that I_{on}/I_{off} ratio equal at least 6 decades independently of processing techniques. Compare to previous results, off-current is reduced and on-current is increased by two decades and one decade, respectively. The low-field effect mobility increases reaching $7 \times 10^{-2} \text{ cm}^2 \text{ V}^{-1} \text{ s}^{-1}$ for spin-coated SU8 OFETs as compared to previous one ($1 \times 10^{-2} \text{ cm}^2 \text{ V}^{-1} \text{ s}^{-1}$). The subthreshold slope improves from 6.5V/Dec to 3.5 V/Dec. Importantly, the contact resistance decreases by more than one decade.

Processing Technique		W/L ($\mu\text{m}/\mu\text{m}$)	Insulator thickness in μm	μ_0 ($\text{cm}^2 \cdot \text{V}^{-1} \cdot \text{s}^{-1}$)	V_{TH} (V)	SS (V/dec.)	R_C (Ω)	V_{DS} (V)
Spin	Average	5000/100	1.5	$7 \cdot 10^{-2}$	29	3.6	$5.4 \cdot 10^5$	20
	Stand. Dev.	--	--	$1.2 \cdot 10^{-2}$	3	0.2	$2.4 \cdot 10^5$	--
IJP	Average	5000/100	1.7	$3.8 \cdot 10^{-2}$	33	3.5	$2.1 \cdot 10^6$	20
	Stand. Dev.	--	--	$0.6 \cdot 10^{-2}$	2.5	0.7	$2 \cdot 10^6$	--

Table 2 represents the two insulator printing conditions (spin coating and inkjet printing) when source and drain contacts are gold evaporated. μ_0 , V_{TH} , subthreshold slope (SS) and Contact resistance R_c are extracted from transfer characteristics using Y-function method described in the text.

If we check the leakage current by making, as previously, a zoom on the starting output characteristics of the OFETs at very low values of the drain-source voltage V_{DS} (**Figure 7c and d**), we found the same negative drain current with more or less the same value if we compare the curves between figures 3 and 7. This means the gate leakage current in SU8 is similar. The difference occurs for the drain-source voltage values when drain current becomes positive. These values in figure 7 are much lower than in figure 3a and 3b. Remembering this drain voltage occurs when the drain electric field is more efficient than the gate electric field, this means the drain electric field is more efficient with evaporated source and drain contacts. It leads to higher drain current as expected from the higher value of the mobility and the lower value of the contact resistance.

This conclusion is confirmed by plotting the starting negative drain current closed to $V_{DS}=0V$ as a function of the gate-source voltage for both types of OFETs. Comparing curves in figures 5 and 8, we observe the starting drain current stays nearly 0 still a higher gate voltage for evaporated source/drain contact OFETs than for printed source/drain contact OFETs. This means we need higher gate-source voltage to compensate the effect of the drain electric field and to get starting negative drain current.

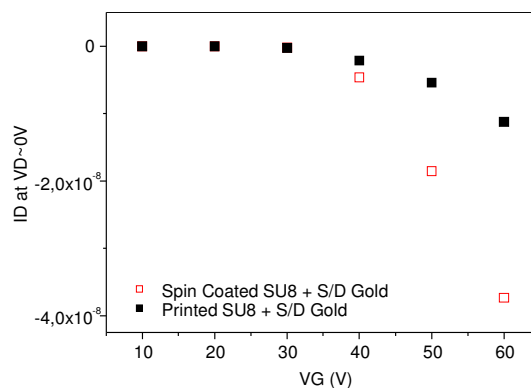


Figure 8: Starting negative drain current (at nearly 0 drain voltage) as a function of the gate voltage. This starting current is derived from the plot of output characteristics at different gate voltage (Figure 8).

Indeed, it is well known that in bottom contact structures, the electrodes engineering is one of the key parameter acting on charge injection into OSC layer.^[36, 38] In particular, thick electrodes disturb the continuous growth of a single-phase domain in active layer.^[39] Moreover, it has also been observed that thick electrodes can also induced

high access resistance due to incomplete step coverage at the contact edge.^[40] Note that, drain and source material can also play a crucial role on OFET electrical behavior.

Conclusion

The ultimate goal of PE is to fabricate fully-printed devices and circuits. However, fully-printed OFET usually shows poorer electrical characteristics than evaporated ones. In this work, OFET structures have been investigated in order to highlight which layer(s) from insulator and drain-source contacts layer have more effect on the electrical parameters. Here, we demonstrate that insulator processing (spin coating or inkjet-printing) technique is not the key parameter which drastically impact the OFET electrical behavior. Indeed, wave-shaped insulator profile induced by coffee ring effect and usually considered as a drawback, is not a limiting factor in order to achieve efficient OFET. However, whatever the insulator deposition technique, the mobility and the on-off current ratio are lower and the contact resistance is higher when using printed source/drain contacts than when using evaporated source/drain contacts. Hypotheses can be drawn to explain this behavior such as: i) the thickness and the morphological difference between printed and evaporated contact, ii) electrodes materials. Consequently, such effects can be considered as limiting factors for fully-printed OFET fabrication. This work has demonstrated that research has to focus on drain and source processing (thickness, morphology, new materials using new inks...) instead of insulator processing. Moreover, this work didn't focus on fully-printed OFET. Indeed, semiconductor has not be printed in order to avoid additional negative effects due to semiconductor drying. Obviously, such effect remains challenging and have to be studied as the impressive work performed by Minemawari et al.^[18]

Methods

Inks processing:

Inks composition: Inks were used without filtering steps. Epoxy based ink (Su8-2000 series; MicroChem, Westborough©, MA, USA) surface tensions and viscosity were 35 mN.m^{-1} and 2.49 cp respectively. Silver nanoparticles (Silverjet DGP 40LT-15C from ANP©) surface tension and viscosity were 35 mN.m^{-1} and 15 cp respectively.

Jettable Criterion. The stroboscopic vision system was used to monitor the following criterion. The jettable criterion is the ability to obtain a droplet at a distance range (Δr) between $800 \mu\text{m}$ and 1 mm (acceptable working distance for the printer equipment: CERADROP© Xseries). Satellite droplets or tail must be reabsorbed by the nozzle and jettability must be stable for a long time with low droplet misalignment on the substrate ($\Delta x < 5 \mu\text{m}$). All the measurements were performed at 1 KHz and 3 kHz jetting frequency for epoxy based ink and silver based ink respectively. Movie S1 and Movie S2 (see supplementary file) shows satisfying and unsatisfying jetting conditions, respectively.

OFET Fabrication steps:

All the printing experiments were performed using CERADROP© X-series printer.

Except the organic semiconducting layer, the OFET devices were fully printed on Corning© glass substrate.

The substrates were ultrasonically cleaned in acetone and isopropyl alcohol for 10 min . Silver gate electrode was printed on glass substrate using 256 nozzles Q-class printhead (Dimatix©) and baked on hot plate at $130 \text{ }^\circ\text{C}$ for 30 min . Then, Epoxy based ink was printed using a 16 nozzles cartridge (Dimatix©) and baked at $95 \text{ }^\circ\text{C}$ for 5 min in an oven followed by UV ($\lambda = 365 \text{ nm}$) exposure and baked again in an oven at $95 \text{ }^\circ\text{C}$ for 5 min . Due to the high hydrophobicity of the insulator, the UV–ozone treatment (Jetlight©) is needed to increase its hydrophilicity allowing the fabrication of accurate drain-source electrodes. Silver source and drain electrodes were printed on a 700-nm -high epoxy layer. Finally, 35-nm -thick organic semiconductor (fullerene C60 Sigma Aldrich©) was thermally evaporated as active layer.

Characterization:

Viscosity and surface tension measurements were monitored using Malvern© labpro+ rheometer and Kruss© DSA30 equipment, respectively. Profilometry measurements were performed using TENCOR© KLA P6 equipment. Optical picture were obtained using binocular vision system equipped with a camera (moticam©). All the electrical tests were performed inside glovebox using Keithley© 2636A and Labview software.

REFERENCES

- [1] P. Calvert, *Chemistry of materials*, 2001, **13**(10), 3299–3305.
- [2] Y. Cho, E. Kim, and W. Kim, *International Journal of Technology Management*, 2015, **67**(2-4), 106–131.
- [3] D. A. Pardo, G. E. Jabbour, and N. Peyghambarian, *Advanced Materials*, 2000, **12**(17), 1249–1252.
- [4] R. R. Søndergaard, M. Hösel, and F. C. Krebs, *Journal of Polymer Science Part B: Polymer Physics*, 2013, **51**(1), 16–34.
- [5] B. Derby, *Journal of the European Ceramic Society*, 2011, **31**(14), 2543–2550.
- [6] M. Singh, H. M. Haverinen, P. Dhagat, and G. E. Jabbour, *Advanced materials*, 2010, **22**(6), 673.
- [7] M. J. Coenen, T. M. Slaats, T. M. Eggenhuisen, and P. Groen, *Thin Solid Films*, 2015, **583**, 194–200.
- [8] F. C. Krebs, *Solar Energy Materials and Solar Cells*, 2009, **93**(4), 394–412.
- [9] M. Medina-Sánchez, C. Martnez-Domingo, E. Ramon, and A. Merkoçi, *Advanced Functional Materials*, 2014, **24**(40), 6291–6302.
- [10] M. Robin, W. Kuai, M. Amela-Cortes, S. Cordier, Y. Molard, T. Mohammed-Brahim, E. Jacques, and M. Harnois, *ACS applied materials & interfaces*, 2015, **7**(39), 21975–21984.
- [11] M. Mionic, K. Pataky, R. Gaal, A. Magrez, J. Brugger, and L. Forró, *Journal of Materials Chemistry*, 2012, **22**(28), 14030–14034.
- [12] H. C. Nallan, J. A. Sadie, R. Kitsomboonloha, S. K. Volkman, and V. Subramanian, *Langmuir*, 2014, **30**(44), 13470–13477.
- [13] B. Derby, *Annual Review of Materials Research*, 2010, **40**, 395–414.
- [14] E. Sowade, K. Y. Mitra, E. Ramon, C. Martinez-Domingo, F. Villani, F. Loffredo, H. L. Gomes, and R. R. Baumann, *Organic Electronics*, 2016, **30**, 237–246.
- [15] S. Gamerith, A. Klug, H. Scheiber, U. Scherf, E. Moderegger, and E. J. List, *Advanced Functional Materials*, 2007, **17**(16), 3111–3118.
- [16] S. Jeong, S. H. Lee, Y. Jo, S. S. Lee, Y.-H. Seo, B. W. Ahn, G. Kim, G.-E. Jang, J.-U. Park, B.-H. Ryu, et al., *Journal of Materials Chemistry C*, 2013, **1**(15), 2704–2710.
- [17] C. Kim, Z. Wang, H.-J. Choi, Y.-G. Ha, A. Facchetti, and T. J. Marks, *Journal of the American Chemical Society*, 2008, **130**(21), 6867–6878.
- [18] H. Minemawari, T. Yamada, H. Matsui, J. Tsutsumi, S. Haas, R. Chiba, R. Kumai, and T. Hasegawa, *Nature*, 2011, **475**(7356), 364–367.

- [19] R. D. Deegan, O. Bakajin, T. F. Dupont, G. Huber, S. R. Nagel, and T. A. Witten, *Nature*, 1997, **389**(6653), 827–829.
- [20] K. Fukuda, T. Sekine, D. Kumaki, and S. Tokito, *ACS applied materials & interfaces*, 2013, **5**(9), 3916–3920.
- [21] I. Etxebarria, J. Tait, R. Gehlhaar, R. Pacios, and D. Cheyns, *Organic Electronics*, 2013, **14**(1), 430–435.
- [22] D. Kim, S. Jeong, B. K. Park, and J. Moon, *Applied Physics Letters*, 2006, **89**(26), 264101.
- [23] J. Chang, X. Zhang, T. Ge, and J. Zhou, *Organic Electronics*, 2014, **15**(3), 701–710.
- [24] J. Kim, B. Lim, K.-J. Baeg, Y.-Y. Noh, D. Khim, H.-G. Jeong, J.-M. Yun, and D.-Y. Kim, *Chemistry of Materials*, 2011, **23**(21), 4663–4665.
- [25] S. H. Ko, H. Pan, C. P. Grigoropoulos, C. K. Luscombe, J. M. Fréchet, and D. Poulikakos, *Nanotechnology*, 2007, **18**(34), 345202.
- [26] B. Kim, S. Jang, M. L. Geier, P. L. Prabhumirashi, M. C. Hersam, and A. Dodabalapur, *Nano letters*, 2014, **14**(6), 3683–3687.
- [27] K.-J. Baeg, D. Khim, D.-Y. Kim, S.-W. Jung, J. B. Koo, I.-K. You, H. Yan, A. Facchetti, and Y.-Y. Noh, *Journal of Polymer Science Part B: Polymer Physics*, 2011, **49**(1), 62–67.
- [28] R. Dufour, A. Dibao-Dina, M. Harnois, X. Tao, C. Dufour, R. Boukherroub, V. Senez, and V. Thomy, *Soft Matter*, 2013, **9**(2), 492–497.
- [29] E. Jacques, M. Romain, A. Yassin, S. Bebiche, M. Harnois, T. Mohammed-Brahim, J. Rault-Berthelot, and C. Poriel, *Journal of Materials Chemistry C*, 2014, **2**(17), 3292–3302.
- [30] R. Dufour, A. Dibao-Dina, M. Harnois, X. Tao, C. Dufour, R. Boukherroub, V. Senez and V. Thomy, *Soft Matter*, 2013, **9**(2), 492–497.
- [31] S. Y. Yang, K. Shin, and C. E. Park, *Advanced functional materials*, 2005, **15**(11), 1806–1814.
- [32] Z. Jian-Lin, Y. Jun-Sheng, Y. Xin-Ge, and C. Xin-Yang, *Chinese Physics B*, 2012, **21**(2), 027305.
- [33] H.-Y. Tseng and V. Subramanian, *Organic Electronics*, 2011, **12**(2), 249–256.
- [34] H. Sirringhaus, T. Kawase, R. Friend, T. Shimoda, M. Inbasekaran, W. Wu, and E. Woo, *Science*, 2000, **290**(5499), 2123–2126.
- [35] J. Wang, Z. Zheng, H. Li, W. Huck, and H. Sirringhaus, *Nature materials*, 2004, **3**(3), 171–176.
- [36] G. Ghibaudo, *Electron. Lett.* 1988, **24**(9), 543–545.
- [37] Y. Xu, T. Minari, K. Tsukagoshi, J. Chroboczek, and G. Ghibaudo, *Journal of Applied Physics*, 2010, **107**(11), 114507.

- [38] G. Horowitz, *Open Applied Physics Journal*, 2011, **4**, 2–7.
- [39] M. Xu, M. Nakamura, M. Sakai, and K. Kudo, *Advanced Materials*, 2007, **19**(3), 371–375.
- [40] T. Richards and H. Sirringhaus, *Journal of Applied Physics*, 2007, **102**(9), 094510.